

Blue supergiants as tests for stellar physics

Cyril Georgy¹, Hideyuki Saio², and Georges Meynet¹

¹ Department of Astronomy, University of Geneva, Chemin Pegasi 51, 1290 Versoix, Switzerland
e-mail: cyril.georgy@unige.ch

² Astronomical Institute, Graduate school of Science, Tohoku University, 980-8578, Japan

ABSTRACT

Context. Massive star evolution is still poorly understood, and observational tests are required to discriminate between different implementations of physical phenomenon in stellar evolution codes.

Aims. By confronting stellar evolution models with observed properties of blue supergiants, such as pulsations, chemical composition and position in the Hertzsprung-Russell diagram, we aim at determining which of the criterion used for convection (Schwarzschild or Ledoux) is best able to explain the observations.

Methods. We compute state-of-the-art stellar evolution models with either the Schwarzschild or the Ledoux criterion for convection. Models are for 14 to 35 M_{\odot} at solar or Large Magellanic Cloud metallicity. For each model, we compute the pulsation properties to know when radial modes are excited. We then compare our results with the position of blue supergiants in the Hertzsprung-Russell diagram, with their surface chemical composition, and with their variability.

Results. Our results at Large Magellanic Cloud metallicity shows only a slight preference for the Ledoux criterion over the Schwarzschild one in reproducing at the same time the observed properties of blue supergiants, even if the Schwarzschild criterion cannot be excluded at this metallicity. We check that changing the overshoot parameter at solar metallicity does not improve the situation. We also check that our models are able to reproduce the position of Galactic blue supergiant in the flux-weighted-gravity – luminosity relation.

Conclusions. We confirm that overall, models computed with the Ledoux criterion are slightly better in matching observations. Our results also support the idea that most Galactic α Cyg variables are blue supergiants of the group 2, i.e. stars that have been through a previous red supergiant phase where they have lost large amount of mass.

Key words. Stars: evolution – Stars: interiors – Stars: massive – Stars: oscillations – Stars: supergiants – Convection

1. Introduction

Although massive stars, progenitors of core-collapse supernovae, play important roles in the chemical evolution of galaxies, their evolution is still poorly understood. Main uncertainties come from our insufficient knowledge of accurate mass-loss rates at various evolutionary stages, the efficiencies of rotational mixing and angular momentum transport, and the range of convective/semi-convective mixing including the extent of overshooting. Constraints to theories for these phenomena should be obtained from comparison of theoretical models with observation. Surface CNO abundances are very useful for constraining theoretical models of rotational mixing in massive stars. Comparison of the surface CNO elements of B stars with theoretical models has been discussed actively (e.g., Hunter et al. 2009; Przybilla et al. 2010; Brott et al. 2011; Maeder et al. 2014; Martins et al. 2015), but there remain some difficulties reconciling theoretical and numerical results with observations, even for main-sequence (MS) stars.

Convection is one of the main transport process to be included in stellar evolution calculations. Despite its importance, it is still poorly understood and its treatment in stellar evolution codes is yet based on very simple models, such as the well known “mixing-length theory” (Böhm-Vitense 1958). Moreover, the position of the convective boundaries relies on one of the stability criterion (either the Schwarzschild criterion or the Ledoux one, see e.g. Maeder 2009). It is known since a long time (e.g. Maeder & Mermilliod 1981) that using either of these criterion

produces too small cores, making mandatory to arbitrary extend the size of the convective cores (this is called the “overshooting”). How this extension has to be done, and what is the efficiency of the mixing of chemical elements throughout the convective boundary (so called “convective boundary mixing”) is so far unknown and largely contributes to our lack of understanding of massive star evolution.

During the last decade, intensive efforts have been started to improve the situation by using three-dimension (3d) hydrodynamics simulation of convection in stellar interior conditions (Meakin & Arnett 2007; Freytag & Höfner 2008; Augustson et al. 2012; Viallet et al. 2013; Müller et al. 2016; Cristini et al. 2017; Mocák et al. 2018, among others). Despite the increasing sophistication and numerical resolution of these simulations, and the powerful insight they allow on stellar convection, we are still far from having new and more precise algorithms to deal with this phenomenon. Some attempts are currently made to include in classical stellar evolution codes lessons learned from 3d hydrodynamics simulations (Scott et al. 2021). To validate these approaches, new observational tests are needed (for example see Tkachenko et al. 2020).

We have been pursuing to obtain constraints to theories by using pulsational properties of blue supergiant (BSG) stars (Saio et al. 2013; Georgy et al. 2014). Blue supergiants are expected to consist of two groups; one group of stars are evolving toward the red supergiant (RSG) stage (group 1 hereafter), the others are returned back from the RSG stage (group 2 hereafter). We distinguish the two groups using the pulsation properties;

BSG stars after RSG show evidence of radial pulsation (α Cyg variables), when BSG evolving from the MS to the RSG branch (first crossing) do not (Saio et al. 2013). We interpreted Deneb (α Cyg) and Rigel (β Ori) as post RSG according to their pulsations which can be reproduced by models which returned to BSG region after losing significant mass during the RSG phase. One puzzle emerged, however: post-RSG models predict surface N/C and N/O ratios much larger than those of Deneb and Rigel, of which N/C and N/O ratios are rather consistent with those of pre-RSG models. The discrepancy indicates that internal mixing was somewhat too strong in our models. Georgy et al. (2014) proposed a possible solution for the problem; i.e., the problem of the surface CNO abundance ratios might be remedied by using the Ledoux criterion in determining the convective/radiative boundaries. However, the latter work focused on only one mass, namely $25 M_{\odot}$, at solar metallicity. In this paper, we intend to extend our previous researches to a broader mass domain and also to the metallicity of the Large Magellanic Cloud (LMC), in order to check if our finding remains valid in other regimes.

Most of the stellar evolution calculations discussed in the literature have been done using Schwarzschild criterion so that discussions of the stellar structure and evolution under the Ledoux criterion are rare in spite that it is not yet understood which criterion should be used. In this paper we first discuss the structure and evolution of massive stars calculated with the Ledoux criterion. Then, we compare observed surface compositions of BSGs with those of models obtained by using the Ledoux or the Schwarzschild criterion. Finally, we revisit the $M_{\text{bol}} - \log g_F$ (luminosity – flux-weighted surface gravity) relation of the BSGs.

2. Massive star models with the Ledoux criterion

As is well known there are two ways to determine the boundary between convection and radiative regions. If the Schwarzschild criterion is employed, convection is assumed to occur if

$$\left(\frac{d \ln T}{d \ln P} \right)_{\text{rad}} > \left(\frac{d \ln T}{d \ln P} \right)_{\text{ad}}, \quad (1)$$

where the temperature gradients with subscripts $_{\text{rad}}$ and $_{\text{ad}}$ indicate the temperature gradient realized if all energy is carried by radiative diffusion (see e.g. Maeder 2009, for the detailed definitions), and adiabatic temperature gradient, respectively. On the other hand, if we adopt the Ledoux criterion, we assume that the convection occurs if

$$\left(\frac{d \ln T}{d \ln P} \right)_{\text{rad}} > \left(\frac{d \ln T}{d \ln P} \right)_{\text{ad}} + \left(\frac{\partial \ln T}{\partial \ln \mu} \right)_P \frac{d \ln \mu}{d \ln P}, \quad (2)$$

where $d \ln \mu / d \ln P$ stands for the gradient of mean molecular weight μ caused by inhomogeneous chemical composition in the stellar interior.

It is known that layers satisfying the Schwarzschild condition (eq. 1) but not the Ledoux criterion (eq. 2) are thermally unstable (overstable; see Kato 1966). This is one of the reasons why the Schwarzschild criterion is preferred in the evolution calculations. It is not clear, however, how efficiently the vibrational thermal instability should mix layers.

Convection in the Geneva stellar evolution code is treated as follows: the limits of convective regions are defined using either the Ledoux or the Schwarzschild criterion. During the main sequence and core helium-burning phase, the convective core is extended by a fraction of $0.1 H_P$, where H_P is the pressure scale height, evaluated at the strict Ledoux or Schwarzschild limit respectively. In this extension of the convective core, the thermal

gradient is assumed to be the adiabatic one. Chemical mixing inside convective zone is assumed to be very efficient and fast compared to the nuclear timescale. The chemical composition is thus homogenised inside convective regions, at least during the first stages of nuclear burning (as is the case for all the models computed in this work).

In this paper, we use different sets of models computed with the Schwarzschild or with the Ledoux criterion. In case the Ledoux one is used, we assume that there is no semi-convection in the regions where the matter is Schwarzschild unstable but Ledoux stable (note however that in case we deal with a model including the effects of rotation, there is a slow mixing of chemical elements inside these regions due to rotational mixing). There are poor constraints on the efficiency of semi-convection in stars, so that we make the decision to compute only extreme cases: pure Ledoux models without semi-convection, mimicking models where semi-convection is very inefficient, and pure Schwarzschild models, corresponding to Ledoux models with infinitely efficient semi-convection. Models with intermediate semi-convective efficiency would fall somewhere in between these two cases (a discussion on the effect of varying the efficiency of semi-convection in massive star models can be found in Kaiser et al. 2020, however in the framework of the MESA code). Let us also emphasise here that the post-MS evolution of massive star is extremely dependent on the detailed mixing scheme adopted in stellar evolution codes, which makes difficult to converge towards firm conclusions (e.g. Higgins & Vink 2019; Schootemeijer et al. 2019).

The stability of radial pulsations is computed in the same way as in Saio et al. (2013). Although the effects of rotation are taken into account in the evolution models, no mechanical effects of rotation are included in calculating the stability of radial pulsations. This is justified because, as discussed in the Appendix in Saio et al. (2013), the rotation speed is always very slow in the envelopes of supergiant stars, to which the amplitude of radial pulsation is confined.

3. Evolutionary models with Schwarzschild and Ledoux criteria for $Z = 0.014$

Fig. 1 shows evolutions of global parameters until the core-helium exhaustion for 20 and $25 M_{\odot}$ models of $Z = 0.014$ (corresponding to a solar metallicity) computed by using the Ledoux (red lines) and Schwarzschild (black lines) criteria. The Geneva evolution code was used as in Saio et al. (2013) and Georgy et al. (2014). Wind mass loss is considered in the same way as described in our previous works (see also Ekström et al. 2012, for more details). In addition to these standard models, and for comparison purpose, we computed three additional models: a $20 M_{\odot}$ computed with the Ledoux criterion and a mass-loss rate multiplied by 2 with respect to our usual mass-loss rates with an initial rotation rate on the zero-age main-sequence (ZAMS) equal to 40% of the critical velocity, and two models of $25 M_{\odot}$ computed with the Ledoux criterion and with an overshoot increased to $0.3 H_P$ (non-rotating and with an initial rotation rate on the ZAMS equal to 40% of the critical velocity).

During the main-sequence evolution, the models with either criteria are nearly identical. This is caused by the following: a) in our models, the chemical composition is initially homogeneous, so that the chemical gradient ∇_{μ} is null everywhere; b) it implies that in the initial models, both criteria lead to the same convective boundary; c) during the MS, the convective core is receding. As the chemical composition inside convective zones is homogeneous, it means that in the convective core,

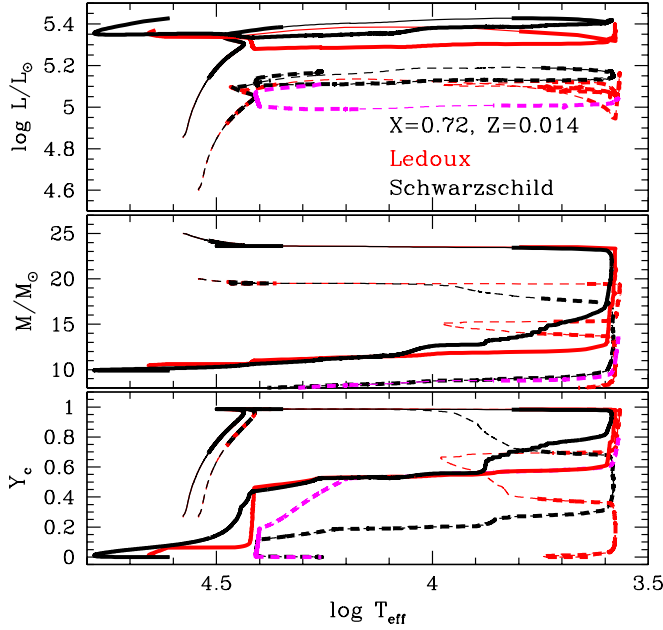


Fig. 1. Evolutionary tracks of 20 (dashed lines) and 25 M_{\odot} (solid lines) models until central helium exhaustion computed with the Ledoux (red lines) and the Schwarzschild (black lines) criteria for the occurrence of convection for an initial composition of $(X, Z) = (0.72, 0.014)$. The magenta line corresponds to the Ledoux 20 M_{\odot} model computed with an enhanced mass-loss rate (2x our standard rates). Top panel is the HR diagram, the middle and the bottom panels show changes in mass and in the central helium abundance, Y_c , respectively, as a function of T_{eff} . Along the thick-line parts radial pulsations are excited.

Schwarzschild and Ledoux criteria coincide, making the models computed with either criterion identical.

During the post main-sequence evolution, the models using the Ledoux criterion are slightly less luminous, but overall evolutions of global parameters are similar irrespective to the convection criteria (note however that the crossing-time of the Hertzsprung-Russell diagram (HRD) can be different, due to the activity of the intermediate H-burning convective zone). After the main-sequence, they evolve to the red supergiant region, where they burn a significant fraction of helium in the core and, at the same time, lose considerable amount of mass. When the helium core occupies about 70% of the total mass, the stars will evolve bluewards, crossing the HRD for the second time (Gianfranco 1967; Farrell et al. 2020). They will thus have another BSG stage, where they consume the remaining helium in the core. Let us mention here that the Ledoux 20 M_{\odot} model at solar metallicity computed with standard mass-loss rates does not lose enough mass during the RSG phase to evolve back to the BSG region of the HRD. As we are interested in stars evolving back to the blue after a RSG phase, we will consider in what follows the Ledoux 20 M_{\odot} with enhanced mass loss: this model is crossing the HRD after its RSG stage and reaches regions in the HRD where the effective temperature corresponds to BSG stars. The Ledoux 20 M_{\odot} model computed with the standard mass-loss rates makes instead a small blue loop and ends its evolution in cooler regions (see red dashed lines in Fig. 1). All the other models discussed in this work are computed assuming the standard mass-loss rates, as in Ekström et al. (2012).

4. Surface abundances of Galactic blue supergiants

4.1. Models with standard parameters

Fig. 2 compares surface N/C and N/O (number) ratios and helium abundances, Y_s (mass fraction) of Galactic blue supergiants with theoretical models with rotation (25 M_{\odot} , blue line and 20 M_{\odot} , black line) and without rotation (25 M_{\odot} , red line). The left panels are for models with the Schwarzschild criterion for convection, while the right panels are for the models with the Ledoux criterion. Radial pulsations are excited in the solid-line parts. Physical parameters of observed BSGs shown here can be found in Table 1 at the end of the article.

The surface helium and CNO abundances in the models after significant mass loss in the red supergiant stage depend strongly on the adopted criterion for convection. As discussed in Georgy et al. (2014) the difference comes from the location of the intermediate convective shell located just above the hydrogen burning shell during the blue supergiant stage evolving toward the red supergiant region (group 1):

Schwarzschild criterion : At the end of the MS, the convective hydrogen-burning core recedes and disappears. Hydrogen burning jumps in a shell located higher inside the star (see the top-left panel of Fig. 3). It creates an associated convective shell which is active enough to sustain the star and prevent a rapid crossing of the HRD. This convective shell is able to transport matter processed by CNO cycle to a high level inside the star. When the star crosses the HRD for a second time towards the BSG region, it has lost a lot of mass during the RSG phase, uncovering layers highly processed by CNO cycle, i.e. with high N/C and N/O ratios.

Ledoux criterion : As in the case of the Schwarzschild criterion, the H-burning convective core disappears at the end of the MS, and the maximum of H-burning migrates at a higher level inside the star. However, it occurs in a region of the star that was previously occupied by the receding H-burning core, and therefore with a non-zero chemical gradient (see the position of the dot-dashed line, which shows the extension of the convective core on the ZAMS : due to H-burning, a chemical gradient is progressively built during the MS below this line). This gradient prevents the appearance of a convective zone at the same depth as with the Schwarzschild criterion. Convection is only able to develop in layers closer to the surface (see the top-right panel of Fig. 3), from where it slowly erodes the chemical gradient, making its lower boundary moving towards the centre of the star. It makes the hydrogen-burning shell much less active compared to the Schwarzschild case, as illustrated in Fig. 4. The luminosity of the shell is not sufficient to sustain the star, which crosses the HRD on a very short timescale : the outer layers expand, a convective envelope appears from the surface and develops in depth, while the intermediate convective shell fades away. The matter inside the intermediate convective shell is less processed compared to the Schwarzschild case, making the N/C and N/O ratios remain smaller at the time when these layers are exposed at the surface because of the mass loss (see Fig. 2). This difference is particularly noticeable in the mass range around 20 to 25 M_{\odot} (higher mass models have a tendency to avoid the red supergiant phase remaining in the blue part of the HRD during the whole evolution, and lower mass models quickly cross the HRD, but don't lose enough mass during the RSG phase to evolve back to the blue later on).

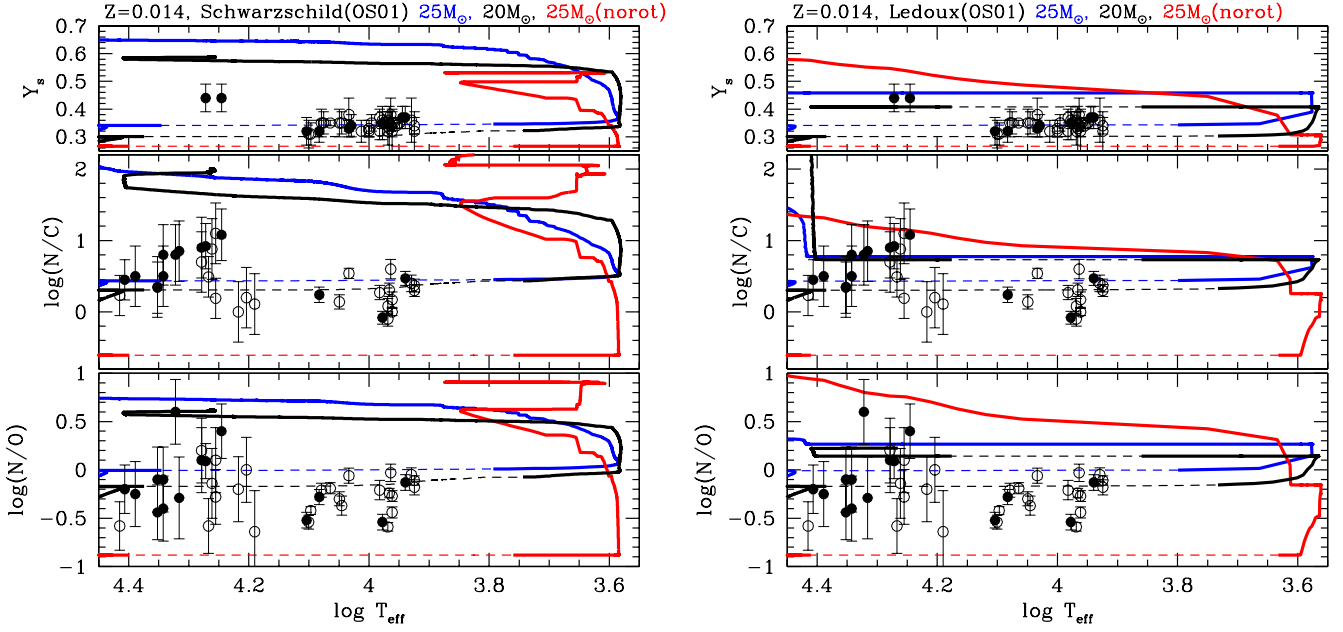


Fig. 2. Surface CNO and helium abundances predicted from $20 M_{\odot}$ (with rotation, black lines) and $25 M_{\odot}$ (with rotation in blue, without rotation in red line) evolutionary models are compared with observed surface CNO and helium abundances of Galactic blue supergiants, where N/C and N/O are number ratios, and Y_s is mass fraction of helium at the surface. Solid parts of the lines indicate where radial pulsations are excited. Filled circles represent α Cyg variables, while open circles are for non-variable BSGs. Left panels are for models with the Schwarzschild condition, while right panels are for models with the Ledoux condition.

For the late B and A type supergiants ($4.15 \gtrsim \log T_{\text{eff}} \gtrsim 3.9$) the surface helium abundances and N/C and N/O ratios are, irrespective to their variability, close to the values of models of the group 1. This is at odds with our explanation of the α Cyg variables as blue supergiants after the red supergiant stages (Saio et al. 2013), in which α Cyg variables should have, in particular for Schwarzschild criterion, higher Y_s , and N/C and N/O ratios. However, for the models with the Ledoux criterion, the discrepancy is considerably reduced since the differences of these quantities for the models before and after the red supergiant stage are much smaller than for the models with the Schwarzschild criterion (Georgy et al. 2014). Due to the much longer time spent on the second crossing compared to the first one (see Table 2), our computations show that there is also a much greater probability to observe a star of the BSG2 group, since the duration of the BSG2 phase is at least 30 times longer than the BSG1 one. The comparison between the tracks and the observation should thus focus on the second crossing.

The surface helium abundance (Y_s) of Galactic early B supergiants ($\log T > 4.15$) are appreciably higher than later B and A supergiants, although only two cases are available; the surface N/C and N/O ratios of the early B α Cyg variables tend to be higher than those of non-variables, in contrast to the case of the late B and A type supergiants. These values of Y_s , N/C , and N/O of the early type α Cyg variables agree with supergiant models returned from the red supergiant stage (group 2) obtained by using the Ledoux criterion, much better than those based on the Schwarzschild criterion. Models with the Schwarzschild criterion predict too high Y_s and N/C values, in particular. Therefore, we conclude that the available spectroscopic surface abundances of Galactic blue supergiants in the literature indicate that the Ledoux criterion is better in reproducing the surface abundances of α Cyg variables, assuming that these stars are group 2 stars as deduced from their pulsational properties. However, despite our

efforts so far, no model seems able to reproduce simultaneously the surface abundances of pulsating late type BSGs and their pulsational properties, even when considering models computed with the Ledoux criterion. Looking at Fig. 2, we could wonder whether Schwarzschild models with lower initial mass could also fit the observed data. However, Schwarzschild models with masses between about $10 M_{\odot}$ to $20 M_{\odot}$ do not show bluewards evolution after the RSG phase (Ekström et al. 2012), unless very high mass-loss rate are considered (Georgy 2012; Meynet et al. 2015a).

In summary : our pulsation models for Galactic metallicity indicates that the only way of reproducing the observed pulsational properties of BSGs is to lose a large amount of mass during a previous RSG stage (Saio et al. 2013). These stars should therefore be members of group 2 BSGs. If this result is correct, then models computed with the Ledoux criterion for convection are in better agreement with the observed surface abundances, even if a perfect match is so far not reached. Also, our findings would indicate that stars with an initial mass of about $20 M_{\odot}$ need a quite high mass-loss rate during the RSG stage to cross the Hertzsprung gap for a second time. This could be achieved in case the current mass-loss prescriptions for RSG are underestimated, or by binary interactions.

4.2. Models with an increased overshoot

The fraction of H_p over which the convective core is extended is a free parameter of the code. The value of $0.1H_p$ generally used in this work is our standard value, and was calibrated by comparing the width of the MS obtained in our calculation with the observed width of MS around $2 M_{\odot}$. It has been suggested that the overshooting as implemented in most stellar evolution code could be mass dependent and increase with the stellar mass

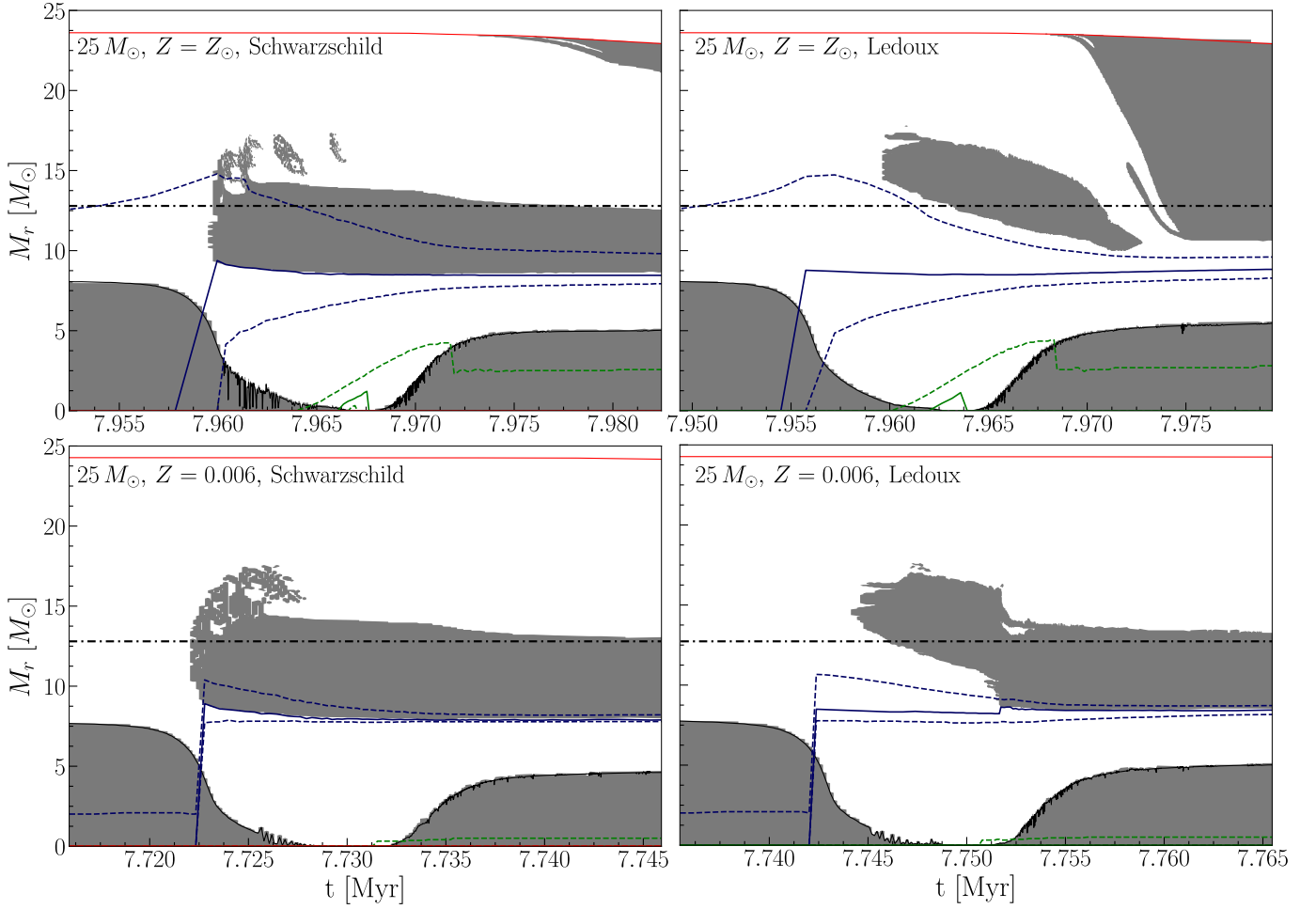


Fig. 3. Kippenhahn diagrams for four representative models of $25 M_{\odot}$: solar metallicity (top row), and $Z = 0.006$ (bottom row); computed with the Schwarzschild criterion (left column) or Ledoux criterion (right column). Grey zones indicate that this part of the star is convective. The mass coordinate of the surface is shown with a red line. Maxima of energy generation rate are indicated for H burning (blue solid line) and He burning (green solid line). The dashed lines indicate, for H and He-burning respectively, the level where the energy generation rate reaches $100 [\text{erg s}^{-1} \text{g}^{-1}]$. The dot-dashed line show the mass-coordinate of the convective core on the ZAMS. It roughly shows the upper boundary of the region in which H-burning has proceeded, and therefore has increased the chemical gradient (due to rotational mixing, the exact extension of the region where a significant chemical gradient is present is slightly larger).

Table 2. Duration of the group 1 BSG^a phase and of the group 2 BSG^a phase for different models computed with the Ledoux criterion for convection. These models have a solar metallicity ($Z_{\odot} = 0.014$)

mass M_{\odot}	rotation $V/V_{\text{crit, ini}}$	comment	BSG1 duration kyr	BSG2 duration kyr
20	0.4	increased \dot{M}_{RSG}	11.5	500.3
25	0.0	-	8.3	306.0
25	0.4	-	6.6	375.1
20	0.4	overshoot $0.3H_P$	6.0	442.4

Notes. ^(a) Here we consider the model as a BSG if he has left the MS and if $3.9 < \log(T_{\text{eff}}) < 4.4$.

(e.g. Castro et al. 2014). In this section, we explore the impact of increasing the fraction to $0.3H_P$ on the properties of BSGs, particularly on their pulsational properties and surface abundances.

On Fig 5 are displayed evolutionary tracks for models computed with the Ledoux criterion for convection ($25 M_{\odot}$ without rotation in red, $25 M_{\odot}$ with an initial rotation rate of 40% of the critical one in blue, and $20 M_{\odot}$ with an initial rotation rate of 40% of the critical one in black). Comparing to the tracks with

standard overshoot (see Fig. 2), the agreement with the observations is slightly worse: particularly, the surface abundance of helium is systematically higher in the models, and the N/O and N/C ratios are also too high in the portions of the tracks where radial pulsations are excited (solid part of the tracks, to be compared with filled circles). The discussion about the duration of the BSG1 and BSG2 phases still holds in this case (see Table 2).

Part of the explanation of this result resides in the bigger core during the MS produced by the increased overshoot. This

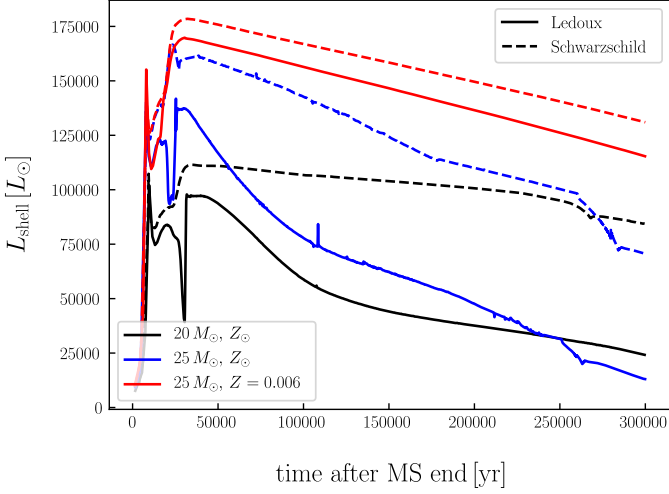


Fig. 4. Time evolution of the luminosity associated with the hydrogen-burning shell during the first couple of 10^5 years after the end of the MS. Solid lines are for models computed with the Ledoux criterion, and dashed lines are for models computed with the Schwarzschild criterion. Black lines are for $20 M_{\odot}$ models at solar metallicity, blue lines for $25 M_{\odot}$ models at solar metallicity, and red lines for $25 M_{\odot}$ models at a metallicity $Z = 0.006$.

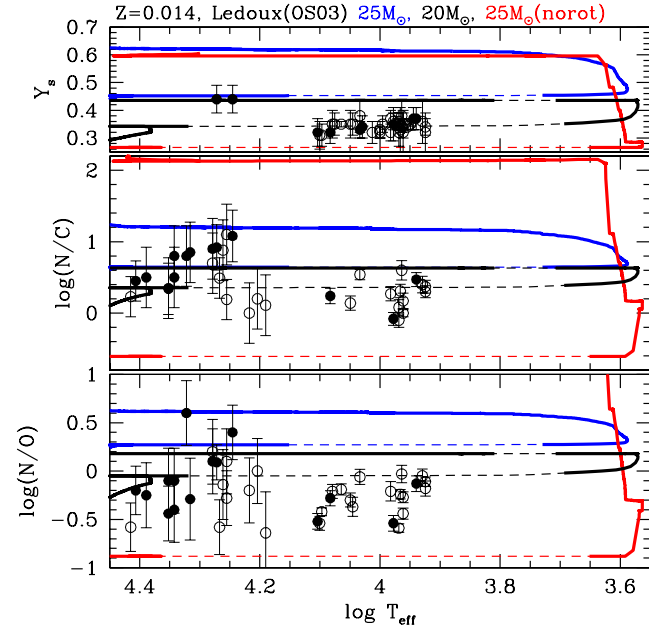


Fig. 5. The same as the right panel of Fig. 2 but for models with an increased overshoot of $0.3H_p$.

reduces the distance between the edge of the convective core (where Y , N/C , and N/O increase as evolution proceeds, due to the CNO cycle) and the surface. As a consequence, the chemical elements produced inside the convective core take a shorter time to reach the surface thanks to rotationnal mixing, making these quantities reaching higher value already during the first crossing of the HRD, and shifting up the overall tracks.

5. Models of massive stars in the LMC

In the previous section, we found that the surface helium and CNO abundances of the Galactic blue supergiants agree with

models based on the Ledoux criterion better than those with Schwarzschild criterion. In this section, we will discuss supergiant models with a LMC composition obtained with the Ledoux and the Schwarzschild criteria.

5.1. Evolution

For the LMC star models, we have adopted a chemical composition of $(X, Z) = (0.738, 0.006)$ (although we have also examined a model with $Z = 0.008$, no qualitative changes occurred). Fig. 6 compares evolution with the Schwarzschild criterion (left panel) and the Ledoux criterion (right panel) for $20 M_{\odot}$, $25 M_{\odot}$, $30 M_{\odot}$, and $35 M_{\odot}$ models. These are rotating models with initial velocity of $0.4 V_c$ (where V_c means the critical rotation speed), except for the green track in right panel, which represents a non-rotating $20 M_{\odot}$ model. Again, thick line parts indicate where radial pulsations are excited.

In contrast to the solar abundance case shown in Fig. 1, Fig. 6 shows that in the case of the LMC composition, core-helium burning tends to occur in a blue region of $4.2 \geq \log T_{\text{eff}} \geq 4$, allowing for a significant amount of mass to be lost in this region of the HRD for models with $M \geq 25 M_{\odot}$. Evolutions with the Ledoux criterion are similar to those with the Schwarzschild criterion when $M \leq 25 M_{\odot}$, while considerable differences occur in more massive cases. In the former case, after a considerable amount of central helium is consumed, the star evolves to the red-supergiant range where core-helium is exhausted.

In the case of the Schwarzschild criterion, 30 and $35 M_{\odot}$ models evolve to red or yellow supergiants after the main-sequence, where they start core-helium burning. After some amount of helium is consumed, they go back to the blue region to finish core-helium burning. In the case of the Ledoux criterion, on the other hand, they start core-helium burning at $\log T_{\text{eff}} \sim 4.2$ without becoming a red or yellow supergiant. The $30 M_{\odot}$ model loses considerable mass during the helium burning and evolves to a red supergiant after most of the central helium is consumed, while the $35 M_{\odot}$ model becomes hotter when it lost more than $10 M_{\odot}$.

The non-rotating model of $20 M_{\odot}$ (green line) with the Ledoux criterion evolves very differently with a long blue loop extending as hot as $\log T_{\text{eff}} \approx 4.6$ after the red supergiant stage, which is rather similar to the cases of the solar metallicity shown in Fig. 1. The model ignites helium burning in the core and consumes significant helium as a red supergiant, during which it loses a mass of about $12 M_{\odot}$. Then it becomes a blue supergiant and consumes remaining helium in the core. This property is however sensitive to the rotation rate; if we include a small initial rotation of $0.2 V_c$, the loop shrinks significantly, extending only to $\log T_{\text{eff}} \approx 3.9$ (not shown in the figure for clarity purpose).

5.2. Distribution of variable and non-variable supergiants of the LMC

Fig. 7 compares the sections of the theoretical tracks where radial pulsations are excited (thick lines) with the observed positions of (semi-) periodic supergiant variables in the LMC (filled symbols). We make the comparison on the HR diagram (rather than the spectroscopic one) because the accurate knowledge of the distance to the LMC make the uncertainties in $\log L$ probably smaller than the uncertainties in $\log g$. Black tracks are for rotating models started with a rotation velocity of $0.4 V_c$. For the case of the Ledoux criterion (right panel), the non-rotating (blue

Table 3. Selected non-LBV supergiant variables in the LMC

HD	$\log T_{\text{eff}}$	$\log L/L_{\odot}^a$	Periods (d)	ref
270920	3.748	5.50	250	1, 2
269018	4.057	5.02	14.6, 6.3, 32.5, 30.2	1, 2
33579	3.890	5.76	105, 81, 57, 70	1, 2
271182	3.775	5.57	260	1, 2
269541	3.877	5.24	8.1, 24.6, 12.0, 40.5	1, 2
269594	3.787	5.16	200	1, 2
269660	4.304	5.84	3.65, 10.8	1, 3
269697	3.797	5.31	48, 84	1, 2
269781	4.005	5.64	39.0	1, 3
268835	4.079	5.44	60, 380	4, 5
37974	4.352	5.90	24	4, 6
268757	3.739	5.42	540	7
268822	3.812	5.15	180	7
269612	3.86	4.93	> 100	7

Notes. ^(a) Luminosities were derived from V magnitudes, assuming a mean extinction of 0.3 mag and a distance modulus of 18.50 mag, and adopting bolometric corrections from Flower (1996).

References. (1) van Leeuwen et al. (1998); (2) McDonald et al. (2012); (3) Urbaneja et al. (2017); (4) van Genderen & Sterken (2002); (5) Stahl et al. (1983); (6) Zickgraf et al. (1985); (7) van Genderen et al. (2004)

line) $20 M_{\odot}$ model and a rotating model with an initial velocity of $0.2V_c$ (red line) are also shown for comparison. On the blue loop of the non-rotating model, radial pulsations are excited because it has lost a significant amount of mass in the previous RSG stage. The excitation of pulsations on the loop seems to contradict the absence of blue variables around the corresponding luminosity. However, due to the sensitivity of the loop to the rotation rate, an initial rotation rate of 20% of the critical rate reduces significantly the loop, removing the discrepancy with the distribution of variable stars on the HR diagram. Since most of the massive stars rotate quite rapidly at this metallicity (most of observed massive stars in the LMC have an equatorial velocity above 100 km/s, Ramírez-Agudelo et al. 2013), we do not consider the long blue loop of the non-rotating model to be a shortcoming of the Ledoux criterion. We consider models with an initial rotation speed above about 20% the critical one to be representative models to be compared with the properties of stars in the LMC: 20% the critical velocity corresponds to an average equatorial velocity of about 125 – 150 km/s during the MS.

In Fig. 7, red filled circles are known LMC α Cyg variables whose parameters are given in Table 3, while the other circles are BSGs in the LMC whose parameters were obtained by Urbaneja et al. (2017). We have examined the variabilities of these BSGs using the Fourier analysis software PERIOD04 (Lenz & Breger 2005) for the G-band lightcurve data from the ASAS-SN database (Shappee et al. 2014; Jayasinghe et al. 2019). Open circles are non-variables, filled magenta circles are probable α Cyg variables showing clear periodicities shorter than ~ 100 days, and filled green circles are stars which marginally show signs of variability. Squares connected with horizontal line are luminous blue variables (LBV), which are included as α Cyg variables, because it is known that the micro-variabilities of LBVs are α Cyg type variations caused by stellar pulsations (e.g. Lamers et al. 1998).

In this figure we see that most of all variables are located either at high luminosity or in a cool enough location of the HRD ($\log T_{\text{eff}} < 3.9$), roughly agreeing with the theoretical prediction for the excitation of radial pulsations irrespective to the convective

criteria employed. For more luminous and hotter stars which have lost considerable mass (see Fig. 6), the pulsations are excited by strange mode instability, while pulsations in less luminous cool stars are excited mainly by the κ -mechanism as in the classical cepheids.

In contrast to our agreement of the LBV micro-variabilities with theoretical prediction of pulsational instability, Lamers et al. (1998) claimed that the microvariations of the LBVs could not be explained by strange-mode instabilities, by comparing models obtained by Kiriakidis et al. (1993) who predicted instability in a region of $\log L/L_{\odot} > 6.0$ for $Z = 0.004$. The discrepancy can be attributed to the difference in the evolutionary models; our models include the effect of rotational mixing which increases the luminosity, and loses a considerable mass during the core-helium burning stage around $\log T_{\text{eff}} \sim 4.2$ (Fig. 6). Both effects increase the luminosity to mass ratio, which in turn enhances the effect of the strange mode instability. The explanation is consistent with the fact that Lovekin & Guzik (2014)’s result based on the old set of Geneva models (Meynet et al. 1994) without rotation indicates that the luminosity at the stability boundary is located between Kiriakidis et al. (1993)’s and ours.

In summary, the distribution in the HRD of the LMC variable/non-variable supergiants does not indicate preference between the Ledoux and the Schwarzschild criteria.

5.3. Surface compositions

Fig. 8 shows the variations of surface helium abundance and CNO ratios during evolutions of 20, 25, 30, and 35 M_{\odot} (magenta, blue, red, and black lines, respectively) with the Schwarzschild (left panel) and the Ledoux (right panel) criteria. The initial rotation speed is assumed to be 40% of the critical speed (V_c). Thick solid lines represent evolutionary stages when radial pulsations are excited, while on the thin dashed line parts no radial pulsations are excited. After the main sequence evolution, in which rotational mixing modifies surface composition, the surface composition start changing at the beginning of the core-helium burning for models massive enough so that the mass loss is significant (the models of 20 M_{\odot} hardly change the surface composition after the end of main sequence, because they lose only a little amount of mass; see Fig. 6). The increase in the surface N/C and N/O ratios and helium abundances are comparable in both cases of the Ledoux and Schwarzschild criteria, in contrast to the case of solar metallicity shown in Fig. 2.

Kippennhahn diagrams are shown in Fig. 3 for the 25 M_{\odot} model with Schwarzschild criterion (bottom left panel) and the one with the Ledoux criterion (bottom right panel). There is no drastic difference in the extension of the convective shell between the two cases, in contrast to the solar metallicity models (top panels of Fig. 3). In both cases, the outer boundary of the shell convection zone extends to about $M_r \approx 18 M_{\odot}$ at the contraction stage after the main sequence evolution. Due to wind mass loss during the core-helium burning stage, the stellar surface reaches the layers where material was previously processed by H-burning. Then the surface N/C and N/O ratios increase steeply. Since the maximum extent of the convective shell is comparable between the models with the Schwarzschild and the Ledoux criterion, the amounts of changes in the surface compositions are comparable in the two cases for models of the LMC composition.

It is not easy to explain the changes in the behaviours of the intermediate H-burning shell at various metallicities and for different criterion for convection. An important point is whether the model starts core-helium burning in the blue part of the HRD or

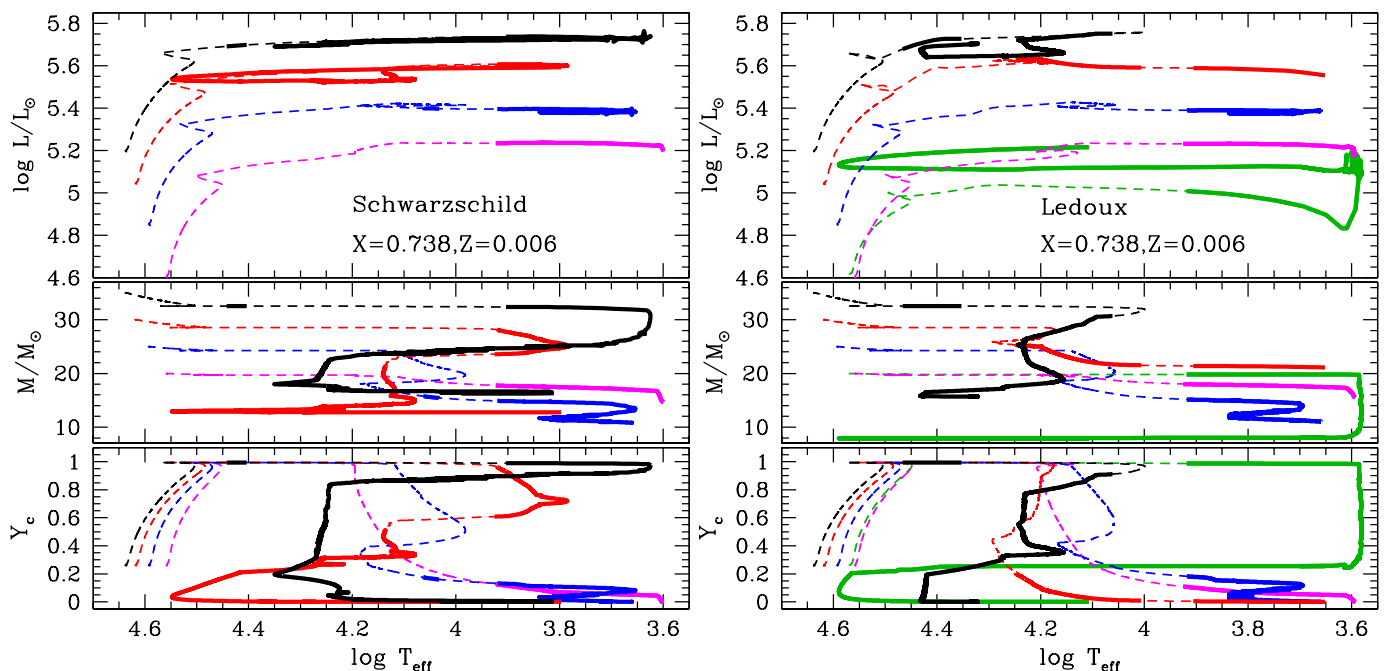


Fig. 6. Models with the LMC composition are shown in the same way as Fig. 1. The initial masses are: 20 (magenta), 25 (blue), 30 (red) and 35 M_{\odot} (black). Left panel shows models computed with the Schwarzschild criterion, and the right one models computed with the Ledoux criterion. The green line shows non-rotating model of 20 M_{\odot} with the Ledoux criterion, while other cases are rotating models with an initial rotation of 0.4 V_c .

crosses the HRD and starts core-helium burning as a RSG. This depends on a variety of parameters, which can be interdependent, such as : rotation (and its implementation), mass-loss rates, chemical gradients in the radiative zones, activity of the intermediate H-burning shell, etc. (Langer & Maeder 1995; Maeder & Meynet 2001). Models at low metallicity tend to remain longer in the blue region of the HRD (e.g. Georgy et al. 2013), and this is also what we observe in the computations used in this work. A similarity between our models at both metallicity is that the luminosity of the hydrogen burning-shell at the onset of shell hydrogen-burning is systematically higher for models computed with the Schwarzschild criterion compared to models computed with the Ledoux one (see Fig. 4). This is due to chemical gradients in the region which was previously occupied by the hydrogen burning-core during the MS (the region below the dot-dashed line in Fig. 3), which prevent a convective zone to appear at the same location where hydrogen is burnt. Hydrogen-shell burning starting in radiative condition with the Ledoux criterion, there is no refueling in fresh hydrogen by convection and then the energy production remains lower. In the Ledoux models, the convective zone appears higher inside the star, where no burning occurs. It then growth at deeper level by eroding the chemical gradient below the convective zone.

The difference between solar and LMC metallicity is that at solar metallicity, the first crossing of the HRD can be fast: all the Ledoux models and the Schwarzschild 25 M_{\odot} models ignite central helium burning on the RSG branch after a quick crossing of the HRD. Only the Schwarzschild 20 M_{\odot} model starts burning its helium as a BSG before slowly crossing the HRD for the first time: the luminosity of the intermediate hydrogen-burning shell is sufficient to maintain the model on the blue side of the HRD, and remains about constant, while in other cases, it decreases over time. Figure 4 shows the time-evolution of the shell luminosity for a couple of 10^5 years after the end of the MS. Three different kinds of behaviour can be seen: 1) models with an abrupt decrease in the shell luminosity short after the shell ig-

nites (Ledoux models at solar metallicity). These are the models which are crossing the Hertzsprung gap very quickly after the end of the MS. 2) models with a slow decrease of the shell luminosity over time (models at $Z = 0.006$ and Schwarzschild solar metallicity 20 M_{\odot} model). These models ignite core-He burning in the blue part of the HRD and cross the gap slowly. 3) model with an intermediate behaviour (Schwarzschild solar metallicity 25 M_{\odot} model). This model is crossing the HRD quite quickly, but not as fast as the models listed in 1). For the models that are quickly crossing the HRD, the intermediate convective zone of the Ledoux models have no time to erode the chemical gradients and to reach the same position as in the Schwarzschild case before the expansion of the external layers switches the intermediate convective zone off. The regions mixed up by convection are thus located at different depth inside the star at this metallicity, changing the surface chemical composition later on, when mass loss uncovers these regions.

At lower metallicity, the luminosity of the hydrogen-burning shell is still higher in the Schwarzschild than in the Ledoux models (see Fig. 4). However this difference is no longer enough for making the Ledoux model crossing quickly the HRD. At this metallicity, core helium-burning starts in the blue part of the HRD in both cases. The convective shell of the Ledoux model appears at a higher level inside the star as shown in Fig. 3 (bottom right panel). Then convection erodes the chemical gradient below the convective zone, which progressively reaches the same position as in the Schwarzschild model, preventing a drop in the luminosity of the intermediate burning shell of the Ledoux models, as can be seen in Fig. 4. The external layers of the star does not expand, keeping the star at quite high effective temperature, and the conditions for keeping an active intermediate convective shell are preserved, contrarily to the solar metallicity case. It leads to a very similar evolution of the intermediate convective shell, independent of the criterion used for convection.

Spectroscopic surface helium abundance, Y_s and CNO ratios of LMC supergiants available in the literature are plotted in

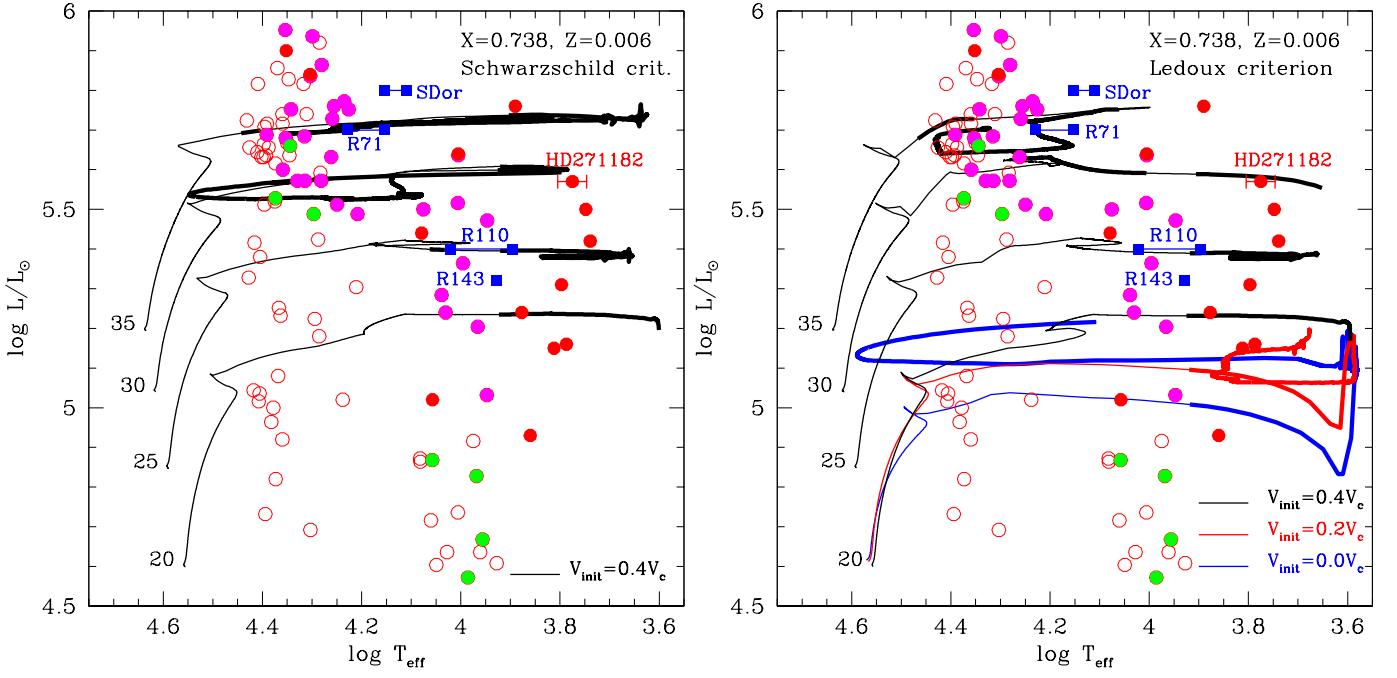


Fig. 7. Evolutionary tracks in the HRD for $Z = 0.006$ with an initial rotation velocity of 0.4 times critical value (black lines), of 0.2 times the critical value (red line), and without rotation (blue line). The left and right panels are for models with the Schwarzschild criterion and the Ledoux criterion, respectively. Thick lines indicate the parts of the tracks where radial pulsations are excited. Also shown are blue supergiants (luminosity classes of Ia, Iab) in the LMC: blue squares connected with horizontal lines are LBVs (S Dor, R 71, R 110, R 143; from brighter to fainter), for which parameters are obtained from Stahl et al. (1990); Lamers et al. (1998); van Genderen (2001). Red filled circles are known LMC α Cyg variables, whose parameters are given in Table 3. The other circles show the positions of BSGs of which parameters were obtained by Urbaneja et al. (2017). The photometric variability of each of these BSGs has been examined using the Fourier analysis software PERIOD04 (Lenz & Breger 2005) for the G-band lightcurve data from the ASAS-SN database (Shappee et al. 2014; Jayasinghe et al. 2019). Based on the analysis we show non-variables by open circles, probable α Cyg variables (with clear periodicities shorter than ~ 100 days) by filled magenta circles, and marginally variables by filled green circles.

Fig. 8. For non-variable supergiants (Ia, Iab), results from the VLT-FLAMES survey (Hunter et al. 2009) are shown; in their analysis the He/H number ratio assumes to be 0.1 (corresponding to $Y_s = 0.285$). These blue supergiants seem to be on the evolution stage just after the main sequence before helium ignition so that the surface N/C and N/O ratios reflect the rotational mixing during the main-sequence stage (we note that if we adopt the Ledoux criterion two stars with highest N/C ratios could be in the core-helium burning stage according to the $30 M_\odot$ model). The N/C ratios of these blue supergiants look comparable (except for one extremely deficient one) with model predictions, while the theoretical predictions of N/O ratios tend to be larger than the observed ratios (see discussion in Maeder et al. 2014).

Very limited spectroscopic results for variable supergiants in the LMC are available; plotted in Fig. 8 are Y_s and N/C, N/O ratios for the LBVs R 71 and R 143 (filled squares) obtained by Lennon et al. (1993) and Mehner et al. (2017); Agliozzo et al. (2019), respectively, and the N/C ratio of the cool α -Cyg variable HD 271182 (filled circle) obtained by Luck & Lambert (1992).

On the HR diagram R 71 and R 143 are located close to the $35 M_\odot$ and $25 M_\odot$ tracks (Fig. 7), corresponding to black and blue lines, in Fig. 8 respectively. This figure indicates that the helium abundances and CNO abundance ratios of R 71 and R 143 are roughly consistent with models either with the Ledoux or Schwarzschild criterion.

For the cool α -Cyg variable HD 271182, only the N/C ratio obtained by Luck & Lambert (1992) is available. On the HR diagram (Fig. 7), HD 271182, which is shown by a filled circle with horizontal error bars, is located along the $30 M_\odot$ track in either

case of Ledoux or Schwarzschild criterion. The surface N/C and the position on the HRD of HD 271182 are consistent only with the model with the Ledoux criterion, but inconsistent with the Schwarzschild criterion. This supports, although only weakly, the Ledoux criterion for the LMC composition. Recently, Neugent et al. (2012) identified many (~ 300) yellow supergiants separating from dominant foreground Galactic dwarfs. We hope that spectroscopic abundance analyses as well as time resolved photometries will be done for these yellow supergiants (luminous ones in particular) in a near future.

To summarize, the properties of BSGs in the LMC do not indicate a clear preference between the Schwarzschild and the Ledoux criterion. In case the evolutionary mass of HD 271182 is correct (about $\sim 30 M_\odot$), then the Ledoux criterion is however better in reproducing the observed characteristics of this star in particular.

6. Flux-weighted gravity–Luminosity Relation

The Flux-weighted gravity–Luminosity Relation was introduced by Kudritzki et al. (2003, 2012) to spectroscopically measure the distances to galaxies. Later, Meynet et al. (2015b) has shown that the relation should be a powerful tool to discriminate between BSG1 and BSG2 because the relation depends on the mass-loss occurred during the stellar evolution. It is thus an important check for our models to compare the predictions of our computations with the observed position of variable BSG in this

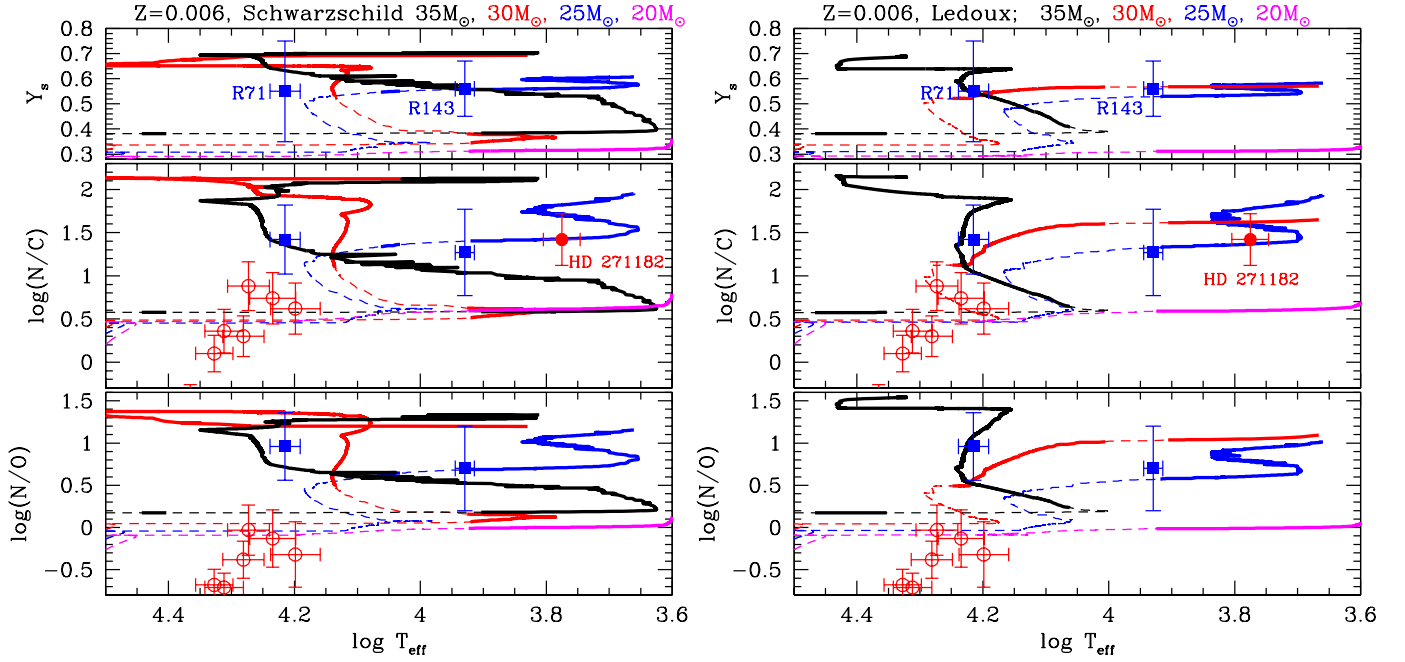


Fig. 8. Evolution of surface chemical compositions of 20, 25, 30, and 35 M_{\odot} models (magenta, blue, red, and black lines, respectively) with the Schwarzschild (left panel) and the Ledoux (right panel) criterion is presented as functions of $\log T_{\text{eff}}$. In those models the initial rotation speed is set to be 40% of the critical value (V_c). Observational results available in the literature for massive LMC stars are also plotted; the meanings of the symbols are the same as in Fig. 7. The chemical compositions of the LBVs (filled squares) are adopted from Lennon et al. (1993) and Mehner et al. (2017) for R 71, and Agliozzo et al. (2019) for R 143. The N/C ratio of the cool α Cyg variable HD 271182 is adopted from Luck & Lambert (1992). Open circles are N/C and N/O ratios of blue supergiants (Ia, Iab) obtained by Hunter et al. (2009); binaries are removed (Maeder et al. 2014).

diagram. The flux-weighted gravities g_F , defined as

$$g_F = \frac{g}{(T_{\text{eff}}/10^4 \text{ K})^4}, \quad (3)$$

of BSGs were found by Kudritzki et al. (2003) to form a tight relation with luminosity (or absolute bolometric magnitude, M_{bol}), where g is the surface gravity and T_{eff} the effective temperature. A most recent calibration is obtained from detailed spectroscopic analysis of blue supergiants in the LMC (Urbaneja et al. 2017). Figure 9 shows the relation with some evolutionary tracks at $Z = 0.006$. The blue line labeled $G2_b$ is the relation corresponding to $\log L/L_{\odot} = 3 \log M/M_{\odot} + 2.03$ obtained by Meynet et al. (2015b) as the lower boundary of the FGLR for BSGs of Local Group galaxies. This figure indicates that the FGLR of LMC is also bounded by the same relation as that of Local Group galaxies.

The positions of the LBVs (filled blue squares) in the $g_F - M_{\text{bol}}$ plane are separated from the mean FGLR towards the lower g_F side. Since $g_F \propto M/L$, the LBV positions indicate that they have lost significantly more mass than the ordinary BSGs, which is consistent with our common understanding of the LBVs. In contrast to the fact that the LBV positions in the HRD are intermingled with the ordinary BSGs (Fig. 7), the segregation of LBVs in the $g_F - M_{\text{bol}}$ plane is remarkable, and could be useful for finding LBV candidates.

Meynet et al. (2015b) discussed on the consistency of the FGLR of Local Group low metallicity galaxies with the theoretical evolution models of Ekström et al. (2012). According to the evolution models, stars whose initial masses are larger than $\sim 20 M_{\odot}$ become BSG for a second time after considerable mass is lost in the red supergiant stage. The BSG2 would be located right side of the $G2_b$ line, and Meynet et al. (2015b) concluded

that the tightness of the FGLR indicates that the evolution towards group 2 BSGs should be rare in local group galaxies. This conclusion is somewhat inconsistent with our identification of α Cyg variables as BSG2s (Saio et al. 2013).

The conclusion of Meynet et al. (2015b) is based on the FGLR of the BSGs in Local Group galaxies. It is more desirable to examine the theoretical and observational consistency using BSGs in our Galaxy. Thanks to the recent second release of the GAIA parallax data, DR2 (Gaia Collaboration et al. 2016, 2018), it is now possible to accurately plot Galactic blue supergiants on the $g_F - M_{\text{bol}}$ plane (Fig. 10). The spectroscopic data of blue supergiants of the Galaxy (see Table 1) needed to obtain g_F are adopted from the literature (Crowther et al. 2006; Searle et al. 2008; Przybilla et al. 2010; Farnstein & Przybilla 2012; Clark et al. 2012). Among the plotted BSG stars, known α Cyg variables are shown by filled circles. For the identifications of the α Cyg type variability, we consulted the literature based on the Hipparcos photometry (Koen & Eyer 2002; Lefèvre et al. 2009; Dubath et al. 2011; Rimoldini et al. 2012).

As seen in Figure 10, the FGLR of the Galactic blue supergiants are similar to that of the LMC, but possibly more extended to the lower g_F side, which may indicate that the blue supergiants in the Galaxy experienced more mass loss than the blue supergiants in the LMC having similar luminosity. This is consistent with the evolution tracks of rotating stars presented by Ekström et al. (2012). Also, it is interesting to note that the loci of the Galactic LBVs in the $g_F - M_{\text{bol}}$ plane (filled blue squares in Fig. 10) are similar ($g_F \sim 10 \text{ cm s}^{-2} (\text{K}/10^4)^4$) to those of the LMC LBVs (Fig. 9) despite the large difference in the metallicity.

In the $g_F - M_{\text{bol}}$ plane, the BSG2s should be located systematically on the lower side g_F side for a given M_{bol} compared

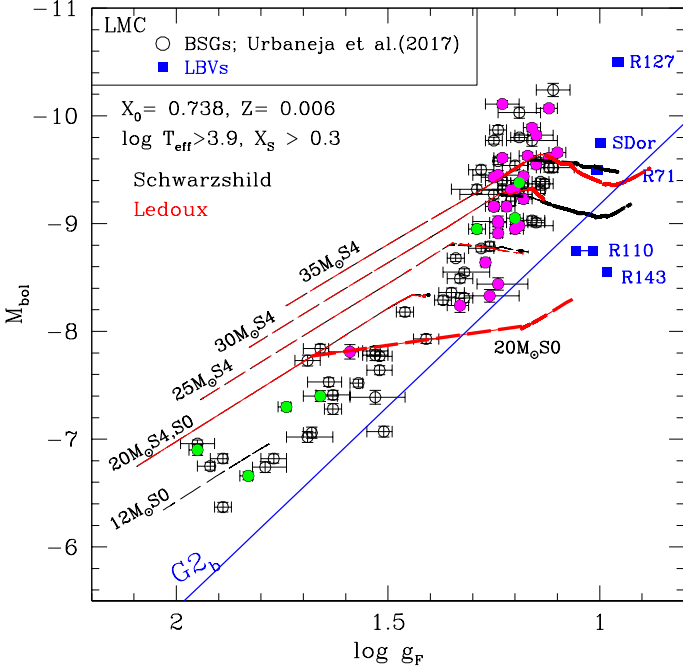


Fig. 9. The LMC blue supergiants analysed by Urbaneja et al. (2017) are plotted by circles in the $\log g_F - M_{\text{bol}}$ plane. The colour of the circles have the same meaning as in Fig. 7. The blue straight line labeled as $G2_b$ is the lower boundary of the FGLR of BSGs in Local group galaxies (Meynet et al. 2015b). Blue parts ($\log T_{\text{eff}} > 3.9$) of some evolutionary tracks with $Z = 0.006$ are also plotted, where thick line parts indicate where radial pulsations are excited. The labels “S0” and “S4” refer to models with an initial rotation rate of 0 and 0.4 of the critical one respectively. Some LBVs are plotted by filled squares for comparison, which clearly indicate that LBVs have experienced significant mass losses.

with the location of BSG1s. The parts of evolution tracks for the BSG2s can be recognized in the right panel of Figure 10 as the (gently ascending) thick-line parts below the $G2_b$ line where radial pulsations are excited. In addition, this figure indicates that radial pulsations are also excited well above the $G2_b$ line if $M \geq 14M_{\odot}$. This is caused by the κ -mechanism in the β -Cep instability strip. As the luminosity increases (i.e., L/M increases), the effect of strange-mode instability gets stronger and the instability range widens to include very luminous α Cyg variables.

In fact, the Galactic α -Cyg variables (red filled circles) are separated into relatively low and very high luminosity groups at $M_{\text{bol}} \sim -9$ (or $\log L/L_{\odot} \sim 5.5$) in the $g_F - M_{\text{bol}}$ plane. The majority of α Cyg variables with $M_{\text{bol}} > -9$ are below the $G2_b$ line in Figure 10, indicating the relatively less luminous α Cyg variables are BSG2s, while there are some very luminous α Cyg variables, which belong to BSG1s.

Since $g_F \propto M/L$, a constant L/M corresponds to a vertical line in the $g_F - M_{\text{bol}}$ diagram. The location of $L/M = 10^4 L_{\odot}/M_{\odot}$ is shown as a red line in Figure 10. A star with $L/M > 10^4 L_{\odot}/M_{\odot}$ should fall in the right side of the vertical line. This figure shows that for the majority of α Cyg variables have $L/M \gtrsim 10^4 L_{\odot}/M_{\odot}$, which indicates that radial pulsations of α Cyg variables are excited by the strange mode instability (e.g. Glatzel 1994; Saio et al. 1998; Saio 2009)¹.

There are some less luminous ($M_{\text{bol}} \gtrsim -6$) stars located below the $G2_b$ line. They cannot be explained by single star evolu-

tions, indicating that transferring a significant envelope mass to a companion in a close binary system would be needed.

7. Conclusion

In this work, we compare models of massive stars computed with both the Schwarzschild and Ledoux criterion with observed pulsating BSGs (α Cyg variables). In particular, we used the position in the HRD, surface chemical composition, excitation of radial modes, and position in the flux-weighted gravity-luminosity diagram to test our models. Confirming our preliminary results (Georgy et al. 2014), our comparisons with observations show the Ledoux criterion is better than the Schwarzschild one at solar metallicity. It improves particularly the fit with the observed surface chemical abundances while keeping a good agreement with the location where radial pulsations are observed in the HRD. This also supports the idea that relatively less luminous ($\log L/L_{\odot} \lesssim 5.5$) Galactic α Cyg variables are group 2 BSGs, i.e. stars that have had a previous RSG stage before crossing the HRD for a second time towards higher effective temperatures. In that case, quite high mass-loss rates during the RSG phase is needed to favour bluewards evolution after the RSG phase.

However, our models still have difficulties in reproducing the surface helium abundance of observed stars, although models computed with the Ledoux criterion are closer to the observations. We also tried to change input physics for convection, by changing the efficiency of the overshoot at solar metallicity. We find that this does not help to improve the agreement between the models and the surface chemical abundances observed in α Cyg variables.

At the LMC metallicity, we show that models produce rather similar results independent of the chosen criterion for convection. This is due to the fact that at this metallicity, changing the criterion does not impact the location where helium-core burning starts in the HRD: it begins in the blue side of the HRD in both cases. Comparison with observations does not strongly favour any of the criterion at this metallicity.

We have compared the FGLR of LMC BSGs (Urbaneja et al. 2017) with our evolutionary tracks. We find that variable BSGs are located in the range of $\log g_F \lesssim 1.4$ (i.e., $L/M \gtrsim 10^4 L_{\odot}/M_{\odot}$). The majority of the LMC BSGs form a relatively tight sequence, which indicates mass losses from them have not been very significant. In contrast, LBVs are located significantly lower g_F side deviating from the tight relation of the other BSGs, which indicates that they have lost significant mass, in agreement with our common understanding of the LBVs.

We also compare the FGLR of Galactic α Cyg variables with the results of our modeling. We find that the FGLR of Galactic BSGs is broader than that of LMC, indicating that wind mass-loss is more active. The FGLR clearly shows that relatively less luminous α Cyg variables are members of group 2 BSGs, while some very luminous α Cyg variables belong to group 1 BSGs.

Our findings suggest that the use of the Ledoux criterion for convection produce slightly better agreements with the observations. More work is needed to confirm this result, since it is probably not independent on other choices made in our models (mass-loss rates, implementation of rotation, implementation of convective boundary mixing, ...). We will continue our efforts to improve the constraints on stellar models that can be deduced from the comparison with observations of BSGs.

Acknowledgements. The authors thank the anonymous referee for her/his valuable comments that contributed to improve this work. This work has made use of data from the European Space Agency (ESA) mission *Gaia* (<https://www.esa.int>).

¹ This also explains the fact that most of the variable LMC BSGs in Fig. 9 are located in the range $\log g_F < 1.4$.

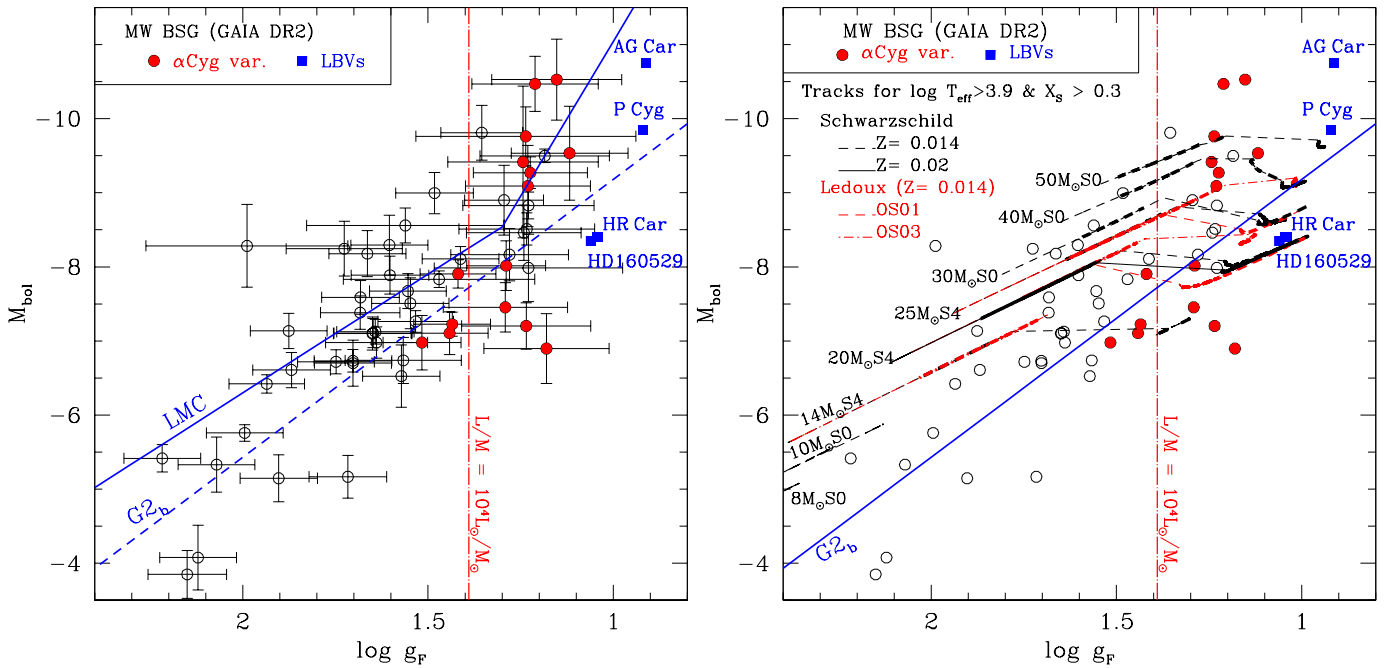


Fig. 10. *Left:* Absolute bolometric magnitudes M_{bol} versus flux-weighted gravity g_F of Galactic blue supergiants are plotted with error bars. For most of the stars GAIA DR2 parallaxes (Gaia Collaboration et al. 2018) are used. A blue line indicates the mean relation of LMC blue supergiants obtained by Urbaneja et al. (2017). Blue dashed line labeled $G2_b$ corresponds to the relation $\log L/L_{\odot} = 3 \log M/M_{\odot} + 2.03$ (Meynet et al. 2015b) which gives the lower bound of the FGLR for the BSGs of Local Group galaxies. *Right:* Blue parts ($\log T_{\text{eff}} > 3.9$) of evolutionary tracks with various parameters are compared. The labels “S0” and “S4” refer to models with an initial rotation rate of 0 and 0.4 of the critical one respectively. Some Galactic LBVs are shown by filled blue squares. The loci on the $g_F - M_{\text{bol}}$ diagram clearly indicate significant mass losses have occurred in LBVs.

cosmos.esa.int/gaia), processed by the *Gaia* Data Processing and Analysis Consortium (DPAC, <https://www.cosmos.esa.int/web/gaia/dpac/consortium>). Funding for the DPAC has been provided by national institutions, in particular the institutions participating in the *Gaia* Multilateral Agreement. CG and GM have received funding from the European Research Council (ERC) under the European Union’s Horizon 2020 research and innovation program (Grant Agreement No. 833925).

References

- Agliozzo, C., Mehner, A., Phillips, N. M., et al. 2019, *A&A*, 626, A126
 Augustson, K. C., Brown, B. P., Brun, A. S., Miesch, M. S., & Toomre, J. 2012, *ApJ*, 756, 169
 Böhm-Vitense, E. 1958, *ZAp*, 46, 108
 Brott, I., Evans, C. J., Hunter, I., et al. 2011, *A&A*, 530, A116
 Castro, N., Fossati, L., Langer, N., et al. 2014, *A&A*, 570, L13
 Clark, J. S., Najarro, F., Negueruela, I., et al. 2012, *A&A*, 541, A145
 Cristini, A., Meakin, C., Hirschi, R., et al. 2017, *MNRAS*, 471, 279
 Crowther, P. A., Lennon, D. J., & Walborn, N. R. 2006, *A&A*, 446, 279
 Dubath, P., Rimoldini, L., Süveges, M., et al. 2011, *MNRAS*, 414, 2602
 Ekström, S., Georgy, C., Eggenberger, P., et al. 2012, *A&A*, 537, A146
 Farrell, E. J., Groh, J. H., Meynet, G., et al. 2020, *MNRAS*, 495, 4659
 Farnstein, M. & Przybilla, N. 2012, *A&A*, 543, A80
 Flower, P. J. 1996, *ApJ*, 469, 355
 Freytag, B. & Höfner, S. 2008, *A&A*, 483, 571
 Gaia Collaboration, Brown, A. G. A., Vallenari, A., et al. 2018, *A&A*, 616, A1
 Gaia Collaboration, Prusti, T., de Bruijne, J. H. J., et al. 2016, *A&A*, 595, A1
 Georgy, C. 2012, *A&A*, 538, L8
 Georgy, C., Ekström, S., Eggenberger, P., et al. 2013, *A&A*, 558, A103
 Georgy, C., Saio, H., & Meynet, G. 2014, *MNRAS*, 439, L6
 Giannone, P. 1967, *ZAp*, 65, 226
 Glatzel, W. 1994, *MNRAS*, 271
 Higgins, E. R. & Vink, J. S. 2019, *A&A*, 622, A50
 Hunter, I., Brott, I., Langer, N., et al. 2009, *A&A*, 496, 841
 Jayasinghe, T., Stanek, K. Z., Kochanek, C. S., et al. 2019, *Monthly Notices of the Royal Astronomical Society*, 485, 961
 Kaiser, E. A., Hirschi, R., Arnett, W. D., et al. 2020, *MNRAS*, 496, 1967
 Kato, S. 1966, *PASJ*, 18, 374
 Kiriakidis, M., Fricke, K. J., & Glatzel, W. 1993, *MNRAS*, 264, 50
 Koen, C. & Eyer, L. 2002, *MNRAS*, 331, 45
 Kudritzki, R. P., Bresolin, F., & Przybilla, N. 2003, *ApJ*, 582, L83
 Kudritzki, R.-P., Urbaneja, M. A., Gazak, Z., et al. 2012, *ApJ*, 747, 15
 Lamers, H. J. G. L. M., Bastiaanse, M. V., Aerts, C., & Spoon, H. W. W. 1998, *A&A*, 335, 605
 Langer, N. & Maeder, A. 1995, *A&A*, 295, 685
 Lefèvre, L., Marchenko, S. V., Moffat, A. F. J., & Acker, A. 2009, *A&A*, 507, 1141
 Lennon, D. J., Wobig, D., Kudritzki, R.-P., & Stahl, O. 1993, *Space Sci. Rev.*, 66, 207
 Lenz, P. & Breger, M. 2005, *Communications in Asteroseismology*, 146, 53
 Lovekin, C. C. & Guzik, J. A. 2014, *MNRAS*, 445, 1766
 Luck, R. E. & Lambert, D. L. 1992, *ApJS*, 79, 303
 Maeder, A. 2009, *Physics, Formation and Evolution of Rotating Stars* (Springer)
 Maeder, A. & Mermilliod, J. C. 1981, *A&A*, 93, 136
 Maeder, A. & Meynet, G. 2001, *A&A*, 373, 555
 Maeder, A., Przybilla, N., Nieva, M.-F., et al. 2014, *A&A*, 565, A39
 Martins, F., Hervé, A., Bouret, J.-C., et al. 2015, *A&A*, 575, A34
 McDonald, I., Zijlstra, A. A., & Boyer, M. L. 2012, *MNRAS*, 427, 343
 Meakin, C. A. & Arnett, D. 2007, *ApJ*, 667, 448
 Mehner, A., Baade, D., Groh, J. H., et al. 2017, *A&A*, 608, A124
 Meynet, G., Chomienne, V., Ekström, S., et al. 2015a, *A&A*, 575, A60
 Meynet, G., Kudritzki, R.-P., & Georgy, C. 2015b, *A&A*, 581, A36
 Meynet, G., Maeder, A., Schaller, G., Schaerer, D., & Charbonnel, C. 1994, *A&AS*, 103, 97
 Mocák, M., Meakin, C., Campbell, S. W., & Arnett, W. D. 2018, *MNRAS*, 481, 2918
 Müller, B., Viallet, M., Heger, A., & Janka, H.-T. 2016, *ApJ*, 833, 124
 Neugent, K. F., Massey, P., Skiff, B., & Meynet, G. 2012, *ApJ*, 749, 177
 Przybilla, N., Farnstein, M., Nieva, M. F., Meynet, G., & Maeder, A. 2010, *A&A*, 517, A38
 Ramírez-Agudelo, O. H., Simón-Díaz, S., Sana, H., et al. 2013, *A&A*, 560, A29
 Rimoldini, L., Dubath, P., Süveges, M., et al. 2012, *MNRAS*, 427, 2917
 Saio, H. 2009, *Communications in Asteroseismology*, 158, 245
 Saio, H., Baker, N. H., & Gautschi, A. 1998, *MNRAS*, 294, 622
 Saio, H., Georgy, C., & Meynet, G. 2013, *MNRAS*, 433, 1246
 Schootemeijer, A., Langer, N., Grin, N. J., & Wang, C. 2019, *Astronomy & Astrophysics*, 625, A132
 Scott, L. J. A., Hirschi, R., Georgy, C., et al. 2021, *arXiv e-prints*, arXiv:2103.06196
 Searle, S. C., Prinja, R. K., Massa, D., & Ryans, R. 2008, *A&A*, 481, 777

- Shappee, B. J., Prieto, J. L., Grupe, D., et al. 2014, *The Astrophysical Journal*, 788, 48
- Stahl, O., Wolf, B., Klare, G., Juettnner, A., & Cassatella, A. 1990, *A&A*, 228, 379
- Stahl, O., Wolf, B., Zickgraf, F.-J., et al. 1983, *A&A*, 120, 287
- Tkachenko, A., Pavlovski, K., Johnston, C., et al. 2020, *A&A*, 637, A60
- Urbaneja, M. A., Kudritzki, R.-P., Gieren, W., et al. 2017, *AJ*, 154, 102
- van Genderen, A. M. 2001, *A&A*, 366, 508
- van Genderen, A. M. & Sterken, C. 2002, *A&A*, 386, 926
- van Genderen, A. M., Sterken, C., & Jones, A. F. 2004, *A&A*, 419, 667
- van Leeuwen, F., van Genderen, A. M., & Zegelaar, I. 1998, *A&AS*, 128, 117
- Viallet, M., Meakin, C., Arnett, D., & Mocák, M. 2013, *ApJ*, 769, 1
- Zickgraf, F.-J., Wolf, B., Stahl, O., Leitherer, C., & Klare, G. 1985, *A&A*, 143, 421

Table 1. Adopted parameters and variability types for Galactic blue supergiants

Name	T_{eff} (K)	$\log(L/L_{\odot})$	$\log g_F$	var	Y_s	$\epsilon(C)$	$\epsilon(N)$	$\epsilon(O)$	Refs
HD 210221	8400±150	4.593±0.063	1.70±0.10	0	0.34±0.03	8.22±0.06	8.52±0.06	8.70±0.05	1
HD 213470	8400±150	5.055±0.108	1.60±0.10	0	0.32±0.07	8.17±0.08	8.54±0.04	8.65±0.03	1
HD 13476	8500±150	4.936±0.096	1.68±0.10	0	0.36±0.08	8.18±0.11	8.58±0.04	8.63±0.06	1
HD 197345	8700±150	4.742±0.124	1.44±0.10	1	0.37±0.04	8.09±0.07	8.56±0.07	8.69±0.04	1
HD 207260	8800±150	4.510±0.188	1.57±0.10	0	0.37±0.04	8.22±0.08	-	-	2
HD 102878	8900±150	4.580±0.134	1.70±0.10	2	0.35±0.02	8.26±0.12	-	-	2,a
HD 165784	9000±200	4.853±0.095	1.68±0.11	0	0.34±0.01	8.39±0.05	-	-	2
HD 91533	9100±150	5.171±0.133	1.66±0.10	0	0.35±0.02	8.20±0.03	-	-	2
HD 14433	9150±150	4.969±0.099	1.55±0.10	0	0.32±0.07	8.23±0.04	8.23±0.03	8.67±0.05	1
HD 111613	9150±150	5.218±0.178	1.60±0.10	0	0.35±0.05	8.29±0.10	8.46±0.04	8.73±0.04	1
HD 12953	9200±200	5.460±0.214	1.29±0.11	0	0.34±0.01	-	8.45±0.03	-	2
HD 195324	9200±150	4.203±0.045	1.99±0.10	0	0.38±0.06	8.10±0.11	8.70±0.08	8.73±0.04	1
HD 207673	9250±100	4.468±0.051	1.93±0.10	0	0.33±0.08	8.17±0.09	8.48±0.03	8.72±0.04	1
HD 80057	9300±150	4.754±0.100	1.88±0.10	0	0.36±0.03	8.24±0.10	8.32±0.04	-	2
HD 187983	9300±250	5.198±0.163	1.73±0.16	0	0.32±0.05	8.29±0.09	8.19±0.04	8.78±0.02	1
HD 14489	9350±250	4.595±0.133	1.57±0.16	0	0.35±0.02	-	8.53±0.06	-	2
HD 13744	9500±250	4.691±0.089	1.64±0.14	0	0.36±0.03	-	-	-	2
HD 92207	9500±200	5.106±0.146	1.29±0.11	1	0.35±0.06	8.33±0.08	8.25±0.04	8.79±0.07	1,b,c
HD 87737	9600±150	3.530±0.196	2.12±0.10	0	0.37±0.03	8.25±0.06	8.52±0.08	8.73±0.06	1
HD 166167	9600±150	4.032±0.164	2.07±0.10	0	0.32±0.03	-	-	-	2
HD 149077	9900±150	4.066±0.075	2.22±0.10	0	0.35±0.03	-	8.45±0.05	-	2
HD 20041	10000±200	4.740±0.093	1.65±0.11	0	0.32±0.02	-	8.30±0.04	-	2
HD 46300	10000±200	3.440±0.140	2.15±0.11	0	0.33±0.03	-	8.43±0.07	-	2
HD 39970	10300±200	4.743±0.082	1.65±0.11	0	0.32±0.04	-	8.15±0.10	-	2
HD 223960	10700±200	5.498±0.119	1.48±0.10	2	0.34±0.04	-	8.55±0.07	-	2,a,c
HD 21291	10800±200	4.691±0.162	1.52±0.10	1	0.33±0.03	-	8.46±0.04	-	2,d
HD 202850	10800±200	3.967±0.123	1.72±0.10	2	0.38±0.06	8.16±0.04	8.70±0.06	8.76±0.05	1,a
HD 149076	11100±200	4.543±0.100	1.87±0.10	0	0.35±0.04	-	8.43±0.09	8.80±0.04	2
HD 212593	11200±200	3.959±0.137	1.90±0.10	0	0.35±0.05	8.30±0.08	8.44±0.06	8.74±0.04	1
HD 106068	11600±200	4.750±0.069	1.64±0.10	0	0.35±0.01	-	8.60±0.04	8.79±0.04	2
BD+602582	11900±200	4.903±0.140	1.55±0.10	0	0.35±0.04	-	8.53±0.05	-	2
HD 105071	12000±150	4.805±0.060	1.53±0.10	2	0.35±0.05	-	8.55±0.06	8.76±0.04	2,b
HD 34085	12100±150	5.062±0.079	1.42±0.10	1	0.32±0.04	8.23±0.09	8.47±0.06	8.75±0.05	1,b
HD 186745	12500±200	5.144±0.068	1.41±0.10	0	0.31±0.04	-	8.35±0.04	8.77±0.01	2
HD 12301	12600±200	4.587±0.067	1.75±0.10	0	0.31±0.05	-	8.14±0.04	8.68±0.06	2
HD 208501	12700±200	4.790±0.067	1.43±0.10	1	0.32±0.05	-	8.24±0.08	8.76±0.01	2,e
HD 164353	15500±1000	5.213±0.258	1.99±0.27	0	-	7.78±0.30	7.89±0.30	8.53±0.30	4
HD 14134	16000±1000	5.305±0.092	1.23±0.18	2	-	8.25±0.30	8.45±0.30	8.45±0.15	3,b
HD 198478	16500±500	5.166±0.151	1.28±0.16	2	-	8.25±0.30	8.25±0.30	8.45±0.15	3,b
HD 152236	17600±500	5.714±0.307	1.12±0.16	1	0.44±0.05	7.69±0.30	8.77±0.20	8.37±0.20	3,5,g
HD 14143	18000±1000	5.431±0.076	1.23±0.18	2	-	7.60±0.30	8.70±0.30	8.60±0.15	3,b
HD 206165	18000±500	5.094±0.192	1.23±0.25	2	-	7.96±0.20	8.15±0.20	8.43±0.20	4,b
HD 14818	18250±500	5.824±0.151	1.36±0.11	2	-	7.66±0.30	8.54±0.30	8.68±0.20	3,4,b
HD 193183	18500±1000	5.323±0.096	1.56±0.27	0	-	7.66±0.20	8.15±0.20	8.73±0.20	4
HD 190603	18700±1000	6.111±0.251	1.15±0.18	1	0.44±0.05	7.84±0.30	8.76±0.10	8.67±0.15	3,4,5,b,e
HD 41117	19000±1000	4.781±0.135	1.23±0.18	1	-	7.65±0.30	8.55±0.30	8.45±0.15	3,b
HD 194279	19000±1000	5.699±0.037	1.18±0.18	0	-	7.95±0.30	8.65±0.30	8.45±0.15	3
HD 13854	20700±2000	5.805±0.164	1.24±0.30	1	-	7.66±0.30	8.51±0.30	8.80±0.30	3,b
HD 14956	21000±1000	6.088±0.164	1.21±0.17	1	-	7.95±0.30	8.75±0.30	8.15±0.15	3,f
HD 91316	22000±1000	4.659±0.215	1.18±0.17	1	-	7.50±0.30	8.30±0.30	8.40±0.15	3,b
HD 148688	22000±1000	5.536±0.258	1.23±0.17	1	-	7.65±0.30	8.15±0.30	8.55±0.15	3,b
HD 2905	22500±1000	4.881±0.144	1.29±0.17	1	-	7.82±0.30	8.16±0.20	8.60±0.20	3,4,b,e
HD 154090	22500±500	5.285±0.165	1.24±0.15	2	-	7.95±0.30	8.30±0.30	8.40±0.15	3,b
HD 91943	24500±500	5.666±0.412	1.24±0.20	1	-	7.65±0.30	8.15±0.30	8.40±0.15	3,b
HD 115842	25500±500	5.608±0.090	1.22±0.15	1	-	7.80±0.20	8.25±0.20	8.45±0.15	3,b
HD 185859	26000±1000	5.033±0.045	1.47±0.26	0	-	7.72±0.20	7.95±0.20	8.53±0.15	4

References. (1) Przybilla et al. (2010); (2) Firnstein & Przybilla (2012); (3) Crowther et al. (2006); (4) Searle et al. (2008); (5) Clark et al. (2012); (a) Koen & Eyer (2002); (b) Lefèvre et al. (2009); (c) Rimoldini et al. (2012); (d) Dubath et al. (2011); (e) ?; (f) ?; (g) ?

^(c) References of (1)–(5) are for physical parameters and surface compositions, and (a)–(g) for the variability types.